CrossMark

ORIGINAL PAPER

Fluorescent Superparamagnetic γ-Fe$_2$O$_3$ Hollow Nanoparticles: Synthesis and Surface Modification by One-Pot Co-precipitation Method

Noshin Mir · Milad Bahrami · Ehsan Safari · S. Mostafa Hosseinpour-Mashkani

Abstract   In this paper, fluorescent superparamagnetic Fe$_2$O$_3$ hollow nanoparticles were successfully synthesized by a template-free one-pot reaction. It was indicated that hollow nanoparticles with 8 nm in size formed in presence of 1,10-phenanthroline (Phen) ligand without employing any hard template, high temperature or additional pressure. Furthermore, various concentrations of the grafting ligand as well as different reaction temperatures were adjusted to identify magnetic properties of the products. An inverse relationship was observed between the amount of the adsorbed ligand and M_{sat} of the prepared sample and it was assessed that ligand concentration and reaction temperature have crucial roles on magnetic properties of the final products. The obtained products were characterized by powder X-ray diffraction, scanning electron microscopy, transmission electron microscopy, vibrating sample magnetometer, Ultra-violet spectroscopy, and photoluminescence spectroscopy. The formation pathway of hollow-shaped nanoparticles is proposed to be due to the special arrangement of the Phen molecules around initial iron oxide nuclei.

Keywords   Superparamagnetic · Co-precipitation · Fluorescent · Optical properties · Iron oxide · Biocompatible nanoparticles

Introduction

Superparamagnetic iron oxide nanoparticles with appropriate surface chemistry are of great interest due to their extensive biomedical applications [1] such as targeted

N. Mir (✉) · M. Bahrami · E. Safari
Department of Chemistry, University of Zabol, PO Box 98615-538, Zabol, Islamic Republic of Iran
e-mail: mir_n84@yahoo.com; n.mir@uoz.ac.ir

S. M. Hosseinpour-Mashkani
Young Researchers and Elites Club, Qom Branch, Islamic Azad University, Qom, Iran

drug delivery [2], magnetic resonance imaging (MRI) [3–5], MRI monitoring in hypothermia [6–8], and selective separation of biomolecules [9, 10]. Therefore, fabrication of developed magnetic nanoparticles (MNPs) by controlling various key aspects such as chemical composition, particle size, and surface properties is quite appealing [11]. To have effective biocompatible magneto-fluorescent nanoparticles, providing a suitable magnetic nanoparticle surface is indispensable to promote the chemical/biological functionalization [12]. In order to modify magnetic nanoparticles, various coating materials such as organic polymers, organic surfactants, inorganic metals, inorganic oxides as well as bioactive molecules and structures are employed [13].

One of the facile and cost-effective chemical synthetic methods for production of MNPs at low temperature (<100 °C) is co-precipitation [11, 14] in which coating procedure is usually performed via a second step after preparation of MNPs [15]. However, there are some reports on the other synthetic methods for one-pot preparation of coated MNPs. Govindaiah et al. [16] prepared 5-amino-1, 10-phenanthroline (APhen)-functionalized luminescent iron oxide nanoparticles via a thermal decomposition process. Aslam et al. [17] proposed a one-step process for synthesis of iron oxide aqueous colloids using the multifunctional molecule dodecylamine (DDA). As biocompatible materials, functionalized MNPs have been recently prepared with intriguing morphologies for further implementation in variety of biological applications such as drug delivery systems. Recent reports have shown diverse strategies for preparation of applicable magnetic structures such as urchin-like nanostructure and hollow spheres. Direct controlled oxidation of MNPs [18], solvothermal [19], and hydrothermal methods [20–22] are some of the well-known means for obtaining hollow-structured MNPs. Though some efforts have been devoted to conduct one-pot template-free synthesis of such structures [23], it still remains a challenging issue. To our knowledge, template-free one-pot co-precipitation method has been rarely reported for synthesis of hollow nanoparticles [24]. Herein, synthesis and characterization of Phen-functionalized γ-Fe_2O_3 nanoparticles with a hollow spherical structure is reported by using a facile one-pot co-precipitation method. Moreover, the magnetic and optical properties of the samples are further investigated.

Materials and Methods

Characterization

$FeSO_4 \cdot 7H_2O$, $FeCl_3$, and 1,10-phenanthroline (Phen) used in our experiments were purchased from Merck. For characterization of the products X-ray diffraction (XRD) patterns were recorded by a Rigaku D-max C III, X-ray diffractometer using Ni-filtered Cu Kα radiation. Scanning electron microscopy (SEM) images were obtained on Philips XL-30ESEM. Transmission electron microscopy (TEM) image was obtained on a Philips EM208 transmission electron microscope with an accelerating voltage of 200 kV. Photoluminescence (PL) spectra were recorded at room temperature with an ArF laser (193 nm) as the excitation source and an iCCD

camera as the detector. The magnetic measurement was carried out in a vibrating sample magnetometer (VSM) (BHV-55, Riken, Japan) at room temperature.

Synthesis of Fe$_2$O$_3$ Hollow Nanoparticles

FeSO$_4$.7H$_2$O and FeCl$_3$ were weighed in the required molar proportion, 1:2. Then, Fe^{3+} was dissolved in deionized water and Fe^{2+} was added to the solution. After a couple of minutes, the precipitation agent, NH$_4$OH was added to the solution with stirring and immediately 1,10-phenanthroline, dissolved in minimum amount of water, was added to the mixture. The pH of the solution was measured to be about 14. The reaction was allowed to proceed for 1 h with constant stirring. Finally, the brown precipitate was washed with ethanol and distilled water and dried at 80 °C for 3 h. The details for reaction conditions of various samples are presented in Table 1.

Results and Discussion

X-ray Diffraction Patterns

The X-ray diffraction patterns of the as-prepared products are shown in Fig. 1. All diffraction peaks can be well indexed to cubic structural γ-Fe$_2$O$_3$. However, it is clearly observed that S4 sample which is prepared at higher temperature is distinctive among the others with sharp peaks showing the high crystallinity of the sample. From XRD data, the crystallite diameter (D_c) of γ-Fe$_2$O$_3$ nanoparticles obtained from sample S1, S2, S3, and S4, were calculated to be 12.49, 18.4, 14.51, and 27.34 nm by using the Scherrer equation, respectively [25]:

$$D_c = K\lambda/\beta \cos \theta \tag{1}$$

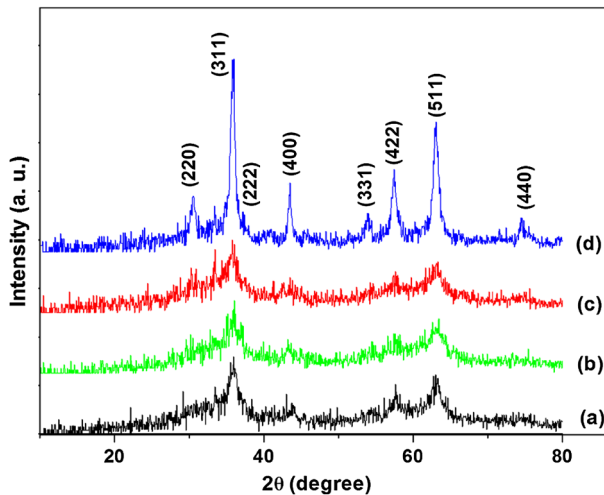where β is the breadth of the observed diffraction line at its half intensity maximum, K is the so-called shape factor, which usually takes a value of about 0.9, and λ is the wavelength of X-ray source used in XRD.

FT-IR Spectroscopy

The as-prepared Phen-functionalized γ-Fe$_2$O$_3$ product was characterized by FT-IR to confirm the organic grafting on its surface. Figure 2a, b show the FT-IR spectra

Table 1 Characteristics of the samples prepared in this work

Sample no.	Fe^{2+}/Phen	Temperature (°C)	Size (nm) (from XRD)	M_{sat} (emu g^{-1}) at RT
S1	1/0.25	25	12.49	55
S2	1/0.5	25	18.40	11
S3	1/1	50	14.51	6
S4	1/1	90	27.34	28

Fig. 1 XRD patterns of the prepared samples: (*a*) S1 (*b*) S2 (*c*) S3 (*d*) S4
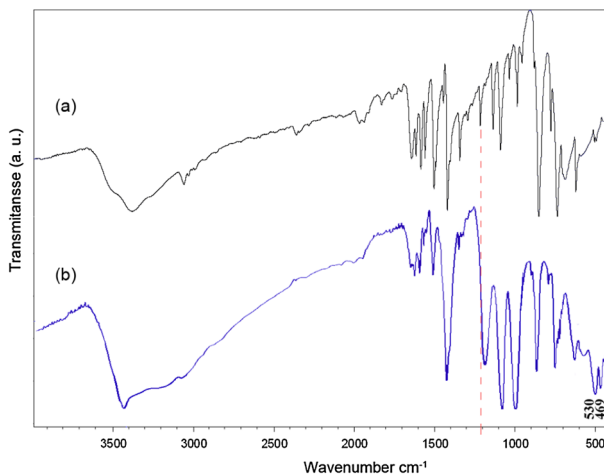
Fig. 2 FT-IR spectra of (*a*) 1,10-phenanthroline (*b*) Phen-functionalized γ-Fe₂O₃ (S4)

of the free 1,10-phenanthroline and Phen-functionalized γ-Fe$_2$O$_3$ (S4), respectively. Maghemite, a defective form of magnetite, has absorption bonds at 590 and 430 cm^{-1} [26]. In Fig. 2b, two absorption bands at 449 and 520 cm^{-1} are assigned to the vibration of the Fe–O bonds. The stretching vibration at 1,310 cm^{-1} in Fig. 2a assigning to aromatic C=N is slightly shifted to lower frequency after grafting on the surface of nanoparticles (Fig. 2b) (marked with the dashed line). Therefore, the adsorption of Phen ligand on the surface of Fe$_2$O$_3$ nanoparticles is approved by FT-IR spectroscopy.

UV–Vis Absorption

Figure 3 shows the UV–vis absorption spectrum of Phen-functionalized γ-Fe$_2$O$_3$ nanoparticles (sample S4). The dispersed nanoparticles in the ethanol shows an absorption band at 300 nm indicating the π–π* intra-ligand transition from the Phen chromophore. In addition, a broad band at 524 nm is attributed to the admixture of the metal to ligand charge transfer (MLCT) of the Phen and iron oxide. The results confirm the functionalization of Phen on to the iron oxide nanoparticles [16].
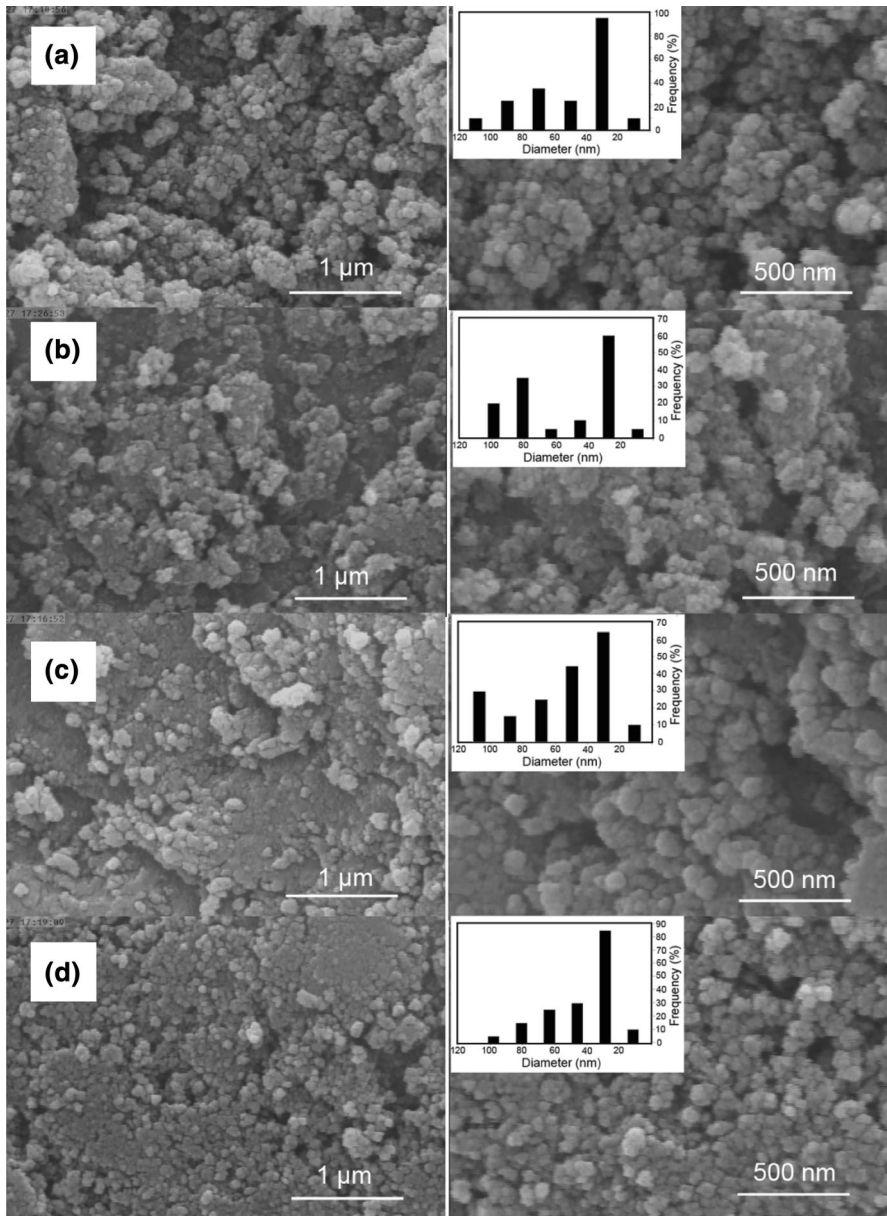
SEM Image

The surface morphologies of the as-prepared products are shown in Fig. 4. It can be observed that although the aggregation size of the particles seems to be over 100 nm, the single particles are tiny. From the SEM images with high magnifications (right-hand images in Fig. 4), the narrowest size distribution belongs to the sample S4 which is prepared at 90 °C. Hence, it can be deduced that the reaction temperature has a crucial effect on nucleation and growth of nanoparticles and it also prevents the particles from haphazard aggregation. The nucleation centres decrease drastically as the temperature increases and low nucleation centres result in large and perfect single crystals [27].

Photoluminescence Properties

Photoluminescence behaviour of one of the as-synthesized samples was investigated and is shown in Fig. 5 which presents room temperature PL spectra of Phen and Phen-coated γ-Fe$_2$O$_3$ samples (S4). It is observed that compared with the pure Phen, the maximum emission wavelength for Phen-coated γ-Fe$_2$O$_3$ nanoparticles (360 nm) is blue-shifted which indicates the deposition of Phen molecules on nanoparticles surfaces [28].
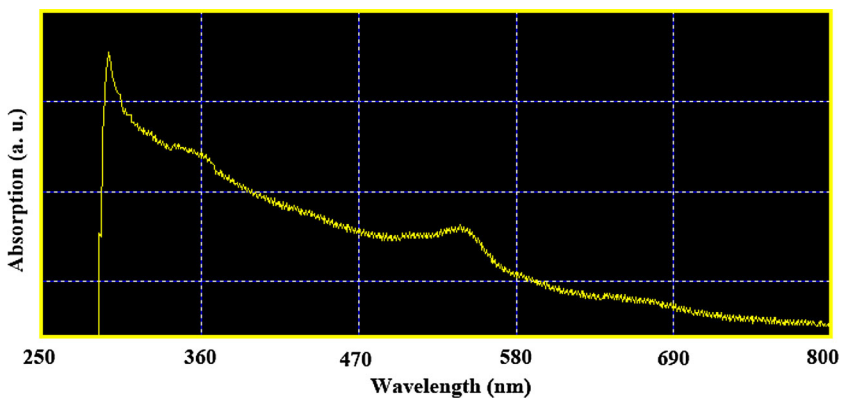

Fig. 3 UV-Vis spectrum of as-prepared Phen-unctionalized γ-Fe$_2$O$_3$ (S4)

Fig. 4 SEM images of the as-prepared products: **a** S1 **b** S2 **c** S3 **d** S4

VSM Analysis

VSM analysis revealed that all the as-prepared samples show the superparamagnetic behaviour at room temperature (Fig. 6). The highest observed M_{sat} is obtained for S1 sample, 55 emu g^{-1}, which is comparable to the best reported values obtained
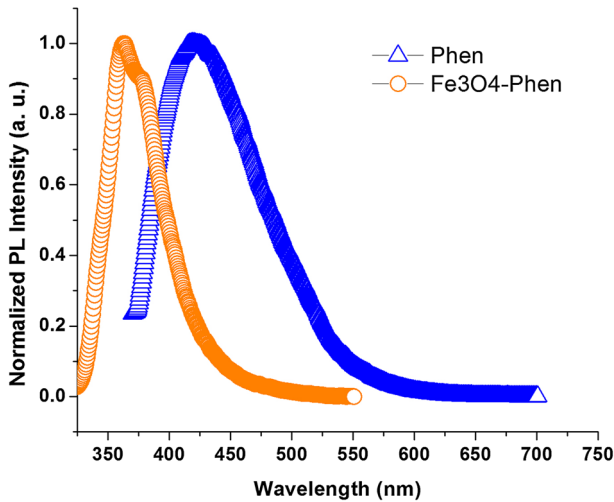
Fig. 5 normalized PL emission of Phen and Phen-unctionalized γ-Fe$_2$O$_3$ (S4) sample

for γ-Fe$_2$O$_3$ nanoparticles [29, 30]. Comparing the magnetic data of the as-prepared samples shows that the M_{sat} value is increased in the following order: S1 > S4 > S2 > S3. The decreased saturation magnetization of the samples is mainly attributed to the different amounts of the surface-anchored functional groups [16]. In this regard, the following observations can be mentioned: (i) increasing Phen concentration lowers the M_{sat} value (S3 < S2 < S1), and (ii) for sample prepared at 90 °C with the highest Phen concentration, M_{sat} is increased due to the increased temperature. It is well-known that high temperature accelerates detaching the anchored molecules from surface [31, 32]. It is deduced that for sample S1, low temperature (25 °C) and low ligand concentration has instigated the reduction of ligand adsorption. Hence, S1 sample shows the most intensified M_{sat}, while S4 stands in the second place. Therefore, in order to have applicable magneto-luminescent nanoparticles, it is crucial to consider both factors i.e. Phen concentration and reaction temperature.

Thus far, the study of magnetic properties as well as morphological characterizations of all samples reveals that S4 sample with the narrowest size distribution and high M_{sat} (28 emu g^{-1}) could be considered the suitable sample for further study. It should be mentioned that although S1 shows higher M_{sat} than S4, the narrow size distribution of S4 compared with S1 was the reason for choosing this sample. Therefore, in this work S4 is known as the optimized superparamagnetic sample and in order to clarify its size, morphology, and crystal structure, it was studied by TEM.

TEM and HR-TEM Images

TEM and HR-TEM images of the sample S4 are shown in Fig. 7. Two different parts of the sample are selected (Fig. 7a, d) and their higher magnifications are shown (Fig. 7b, c, e, f, respectively). The images show agglomeration of
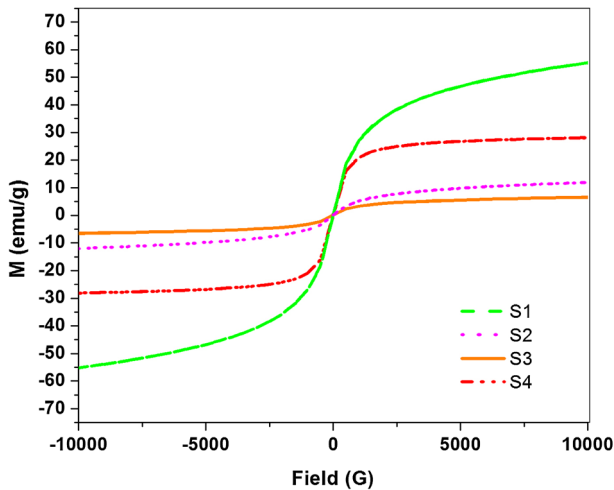
Fig. 6 Magnetization versus magnetic field applied at 25 °C for the as-prepared products

nanoparticles which is because of the applied aqueous route that suffers from less-uniform sizes and size distributions due to the agglomeration induced by the existence of surface hydroxyls [33]. Moreover, since no long chain surfactant is used in this process, the magnetic interaction of naked particles as well as their tiny size with large surface areas increase the tendency of particles for accumulating. From TEM image shown in Fig. 7a, it is observed that nanoparticles show spherical shapes with the average size of 8 nm which is quite different from that of indicated by the previous XRD measurement. The contradiction may be due to the fact that Scherrer formula does not take the presence of a passivation layer or surface structural defects and surface strains into account [34]. The size distribution diagram presented in inset of Fig. 7a shows that the particle size is pretty uniform with a normal size distribution of particles between 5 and 10 nm. The magnetic diameter is generally smaller than the diameter obtained by TEM. This feature is generally attributed to the presence of defects that contributes to formation of less-ordered layer on the particle surface [34]. Figure 7b, e show the higher magnification of nanoparticles as well as the selected area diffraction (SAED) pattern which indicates polycrystalline structure of nanoparticles. It is observed that both images show hollow nanoparticles which are agglomerated. In Fig. 7b, c, nanoparticles are undamaged and therefore only the spherical shapes with hollow morphologies are recognized. However, in HR-TEM images (Fig. 7e, f) a broken nanoparticle is illustrated in which both the hollow centre and edges are visible.
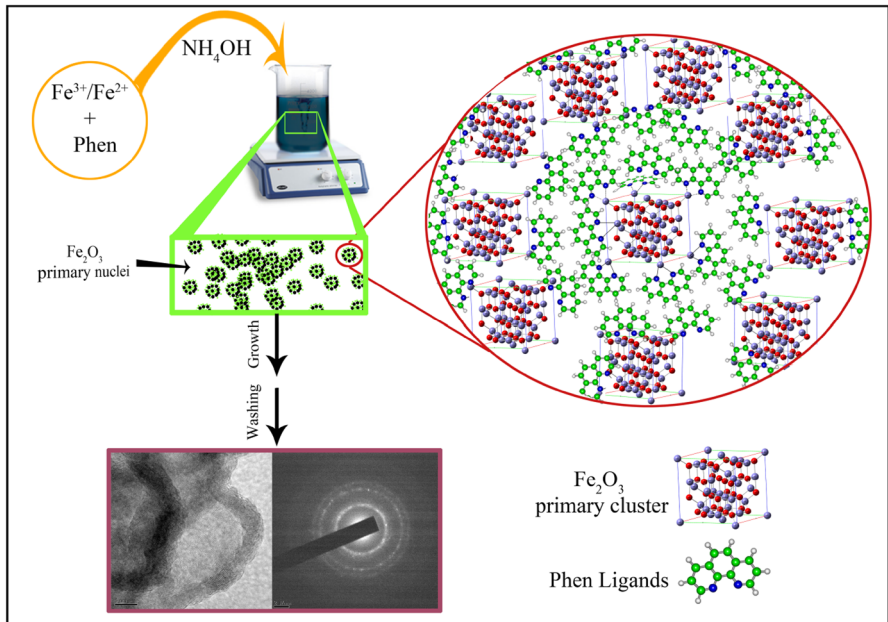
Proposed Formation Mechanism

Based on the obtained results and the observed morphology in TEM images, a formation mechanism is proposed. Since no specific template is employed in the synthesis of the hollow structures, it is assumed that creation of the initial nuclei for further formation of hollow shapes should be due to the special arrangement of the
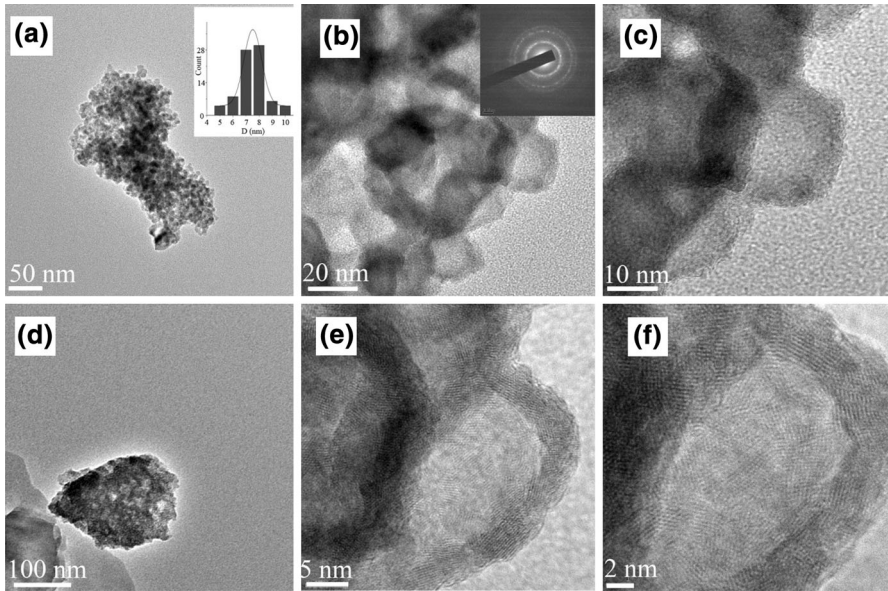
Fig. 7 **a–e** TEM images, size-distribution function, and SAED pattern, **e**, **f** HRTEM images of sample S4

Scheme 1 Proposed formation mechanism for hollow Phen-unctionalized γ-Fe₂O₃ nanoparticles

Phen molecules. Scheme 1 presents the proposed schematic microscopic view of how the formation pathway of hollow structures is supposedly conducted. While the Phen ligand is simultaneously added with iron salts, Fe_2O_3 network forms right after addition of NH_4OH solution. Phen ligands, having N chelating atoms with high affinity toward Fe cations, will be instantly attached to the on-forming Fe_2O_3 primary nuclei and their bulky hydrocarbon structures arrange in the opposite direction. This arrangement which presumably looks like the configuration illustrated in Scheme 1 (the enlarged oval), may cause the nuclei to grow in a special figure, forming the final hollow-shaped nanoparticles.

Conclusions

A facile one-pot co-precipitation method was employed to prepare the hollow-structured γ-Fe_2O_3 nanoparticles. Magnetic and optical properties revealed that both the concentration of Phen and the reaction temperature play important roles on achieving the best magneto-luminescent nanoparticles. It was shown that the sample prepared at 90 °C with 1:1 molar ratio of ligand to Fe^{2+} is the best sample in magnetic property. HR-TEM studies showed that the selected sample shows hollow structure which has potential biological applications. From magnetic data obtained for various samples, it is observed that the M_{sat} value is increased in the order of S1 > S4 > S2 > S3.

References

1. C. Xu and S. Sun (2013). *Adv. Drug. Deliver. Rev.* **65**, 732.
2. S. A. Wahajuddin and S. Arora (2012). *Int. J. Nanomed.* **7**, 3445.
3. A. Senpan, S. D. Caruthers, I. Rhee, N. A. Mauro, D. Pan, G. Hu, M. J. Scott, R. W. Fuhrhop, P. J. Gaffney, S. A. Wickline, and G. M. Lanza (2009). *ACS Nano.* **3**, 3917.
4. H. Basti, L. B. Tahar, L. S. Smiri, F. Herbst, M. J. Vaulay, F. Chau, S. Ammara, and S. Benderbous (2010). *J. Colloid Interface Sci.* **341**, 248.
5. B. Xu, H. Dou, K. Tao, K. Sun, J. Ding, W. Shi, X. Guo, J. Li, D. Zhang, and K. Sun (2011). *Langmuir* **27**, 12134.
6. Y. Hu, L. Meng, L. Niu, and Q. Lu (2013). *ACS Appl. Mater. Interfaces* **5**, 4586.
7. M. D. Shultza, S. Calvin, P. P. Fatouros, S. A. Morrison, E. E. Carpenter, and J. Mag (2007). *Mag. Mater.* **311**, 464.
8. A. A. Elsherbini, M. Saber, M. Aggag, A. Shahawy, and H. A. Shokier (2011). *Magn. Reson. Imaging* **29**, 272.
9. J. C. Liu, P. J. Tsai, Y. C. Lee, and Y. C. Chen (2008). *Anal. Chem.* **80**, 5425.
10. J. Wang, A. Munir, Z. Zhu, and H. S. Zhou (2010). *Anal. Chem.* **82**, 6782.
11. H. Shokrollahi (2013). *Mater. Sci. Eng. C* **33**, 4485.
12. Z. Karimi, L. Karimi, and H. Shokrollahi (2013). *Mater. Sci. Eng. C* **33**, 2465.
13. O. Veiseh, J. W. Gunn, and M. Zhang (2009). *Adv. Drug. Deliv. Rev.* **62**, 284.
14. A. Umara, M. S. Akhtar, G. N. Dar, and S. Baskoutas (2013). *Talanta* **116**, 1060.
15. J. Fouineau, K. Brymora, J. M. Greneche, L. Ourry, F. Mammeri, N. Yaacoub, F. Calvayrac, and S. Ammar-Merah (2013). *J. Phys. Chem. C* **117**, 14295.

16. P. Govindaiah, T. J. Park, Y. J. Jung, S. J. Lee, D. Y. Ryu, and J. H. Kim (2010). *Macromol. Res.* **18**, 1109.
17. M. Aslam, E. A. Schultz, T. Sun, T. Meade, and V. P. Dravid (2007). *Cryst. Growth Des.* **7**, 471.
18. K. Cheng, S. Peng, C. Xu, and S. Sun (2009). *J. Am. Chem. Soc.* **131**, 10637.
19. Y. Chen, H. Xia, L. Lu, and J. Xue (2012). *J. Mater. Chem.* **22**, 5006.
20. I. Opačak, M. Ristić, and S. Musić (2010). *Mater. Lett.* **64**, 2555.
21. G. Gao, P. Qiua, Q. Qianb, N. Zhoua, K. Wanga, H. Songa, H. Fua, and D. Cui (2013). *J. Alloys Compd.* **574**, 340.
22. S. W. Cao, Y. J. Zhu, M. Y. Ma, L. Li, and L. Zhang (2008). *J. Phys. Chem. C* **112**, 1851.
23. L. Li, Y. Chu, Y. Liu, and L. Dong (2007). *J. Phys. Chem. C* **111**, 2123.
24. F. Meng, J. Yin, Y. Q. Duan, Z. H. Yuan, and L. J. Bie (2011). *Sensors Actuators B* **156**, 703.
25. H. P. Klug and L. F. Alexander *X-ray Diffraction Procedures for Polycrystalline and Amorphous Materials*, 2nd ed (Wiley, New York, 1974), pp. 687–692.
26. H. Namduri and S. Nasrazadani (2008). *Corros. Sci.* **50**, 2493.
27. M. R. Shedama and A. Venkateswara-Rao (1998). *Mater. Chem. Phys.* **52**, 263.
28. Z. G. Wang, X. T. Zu, S. Zhu, X. Xiang, L. M. Fang, and L. M. Wang (2006). *Phys. Lett. A* **350**, 252.
29. M. Singh, P. Ulbrich, V. Prokopec, P. Svoboda, E. Šantavá, and F. Štěpánek (2013). *J. Magn. Magn. Mater.* **339**, 106.
30. S.-W. Cao, Y.-J. Zhu, M.-Y. Ma, L. Li, and L. Zhang (2008). *J. Phys. Chem. C* **112**, 1851.
31. T. E. M. ten Hulscher and G. Cornelissen (1996). *Chemosphere* **32**, 609.
32. M. D. McGlamery and F. W. Slife (1966). *Weeds* **14**, 237.
33. X. Liang, X. Wang, J. Zhuang, Y. Chen, D. Wang, and Y. Li (2006). *Adv. Funct. Mater.* **16**, 1805.
34. N. T. K. Thanh *Magnetic Nanoparticles: From Fabrication to Clinical Applications* (CRC Press, Boca Raton, 2012).